IEEE Access
Multidisciplinary | Rapid Review | Open Access Journal

Received May 26, 2020, accepted June 2, 2020, date of publication June 8, 2020, date of current version June 18, 2020.

Digital Object Identifier 10.1109/ACCESS.2020.3000665

Green Traffic-Oriented Heavy-Duty Vehicle Emission Characteristics of China VI Based on Portable Emission Measurement Systems

YINGSHUAI LIU[1,2] AND JIANWEI TAN[2]

[1]Weifang University of Science and Technology, Weifang 262700, China
[2]National Laboratory of Auto Performance and Emission Test, School of Mechanical and Vehicular Engineering, Beijing Institute of Technology, Beijing 100811, China

Corresponding author: Yingshuai Liu (liuyingshuai1983@163.com)

This work was supported by the National Natural Science Foundation of China under Grant 51508304 and Grant 41275133.

ABSTRACT With a continuous increase in vehicle ownership, vehicle emissions have become one of the main sources of air pollution in China. Serious air pollution is a great threat to human health and life. The China VI regulations, which adopt strict particulate matter (PM) and nitrogen oxide (NO_x) limitations, have been implemented. As one of the best technologies for measuring vehicle emissions, portable emission measurement systems (PEMSs) have gained attention. In this work, the characteristics of China VI heavy-duty vehicle emissions were investigated with a PEMS. The effects of road conditions on NO_x, hydrocarbon (HC), carbon monoxide (CO), PM and particle number (PN) pollutants were analyzed based on distance-based emission factors. The results show that the gaseous pollutant levels of NO_x, HC and CO for China VI vehicles are much lower than those for China V vehicles. The average distance-based emission factors of NO_x CO and HC decreased by 88%, 98%, and 62.7%, respectively. Based on the power-based window method, the PEMS test results for NO_x, HC and CO are 460 mg·(kWh)$^{-1}$, 192 mg·(kWh)$^{-1}$ and 37.5 mg·(kWh)$^{-1}$, respectively. According to the PEMS tests, approximately 88%–95% of the particles are in the 10–100 nm class based on three typical operational modes, which represent approximately 0.08%–0.13% of the total particle mass. These heavy-duty vehicles can satisfy the requirements of the PEMS China VI standards. This study emphasizes the importance of obtaining real-world measurements of heavy-duty vehicles to improve the accuracy of emission factors in the development of emission inventories in China.

INDEX TERMS Heavy-duty vehicles, PEMS, emission factor, China VI, emission characteristics.

I. INTRODUCTION

China will nationally implement the China VI emission standards in July 2021; the standards in the Beijing, Tianjin and Hebei area, Pearl River Delta region, and Chengdu-Chongqing region will be implemented in July 2019 [1]–[3]. Compared with the China V emission standards, the emission limits of nitrogen oxide (NO_x) and particulate matter (PM) were restricted by 77% and 67%, respectively, in the new standard, and particle number (PN) limits were added [4]–[6]. The China VI standards for heavy-duty diesel engines combine the advanced aspects of the European Emission standards and North American Emission standards and include more stringent requirements according to the actual situation in China [7]–[9]. The China VI emission standards for heavy-duty diesel are among the most stringent emission standards in the world [10]–[12]. Because the test loop emission results of engine bench tests cannot reflect actual vehicle emissions, European and American countries have begun to use a portable emission measurement system (PEMS) to measure the practical emissions of vehicles, offset the shortcomings of engine bench tests and detection loop tests, and comprehensively and practically determine the vehicle real emission level [13], [14]. The PN was introduced in this standard, and the emission durability, on-board diagnostics (OBD) level and other related

The associate editor coordinating the review of this manuscript and approving it for publication was Guangdong Tian.

requirements have become stricter; moreover, PEMS test requirements were introduced [15]–[17]. The total emissions of carbon dioxide (CO_2), hydrocarbon (HC), NO_x and PM from heavy vehicles are 8.613 million tons, 1.237 million tons, 4.343 million tons and 0.373 million tons, respectively, each year, which account for 30.1%, 37.9%, 83.2% and 88.4%, respectively, of the total emissions of vehicles, which are the main contributors to vehicle emissions.

Unlike traditional engine bench test methods, PEMS technologies require only installation of the related test instrument on the assigned vehicle to perform practical emission tests rather than laboratory tests after disassembling an engine. This method not only saves considerable time and resources but also allows real-time data to be obtained for the first time [18], [19]. With the widespread application of PEMS technologies, vehicle emissions will develop from the single engine bench test method to the combination of engine bench tests with PEMS technologies [20], [21].

Currently, PEMS technology-related studies are being conducted around the world. A West Virginia University (WVU) study applied a PEMS to conduct emission tests of three diesel vehicles in use [22]. Based on the PEMS, Merkisz *et al.* of Poznan University of Technology measured the emissions of tail gas in different road and environmental conditions for a gasoline-natural gas dual-fuel vehicle that satisfies the Euro V emission standards [23]. Park *et al.* of South Korea's National Environmental Research Institute selected 12 light diesel vehicles that satisfy the Euro 3-5 emission standards for measuring NO_x emissions from the NEDC cycle of light-duty diesel vehicles with a laboratory chassis dynamometer [24]. Kean *et al.* analyzed California's non road mechanical emissions based on fuel consumption. PM and NO_x emissions in California were estimated [25]. Researchers in China have also performed a substantial amount of work on PEMS testing. Shen *et al.* from Beijing Technology and Business University employed a SEMTECH-DS vehicle-mounted test system and 3 agricultural vehicles to implement practical road driving tests; they determined the average emission factors of HC, NO_x, CO and CO_2 based on fuel consumption [19]. Guo *et al.* utilized portable vehicle emission test systems to test the actual road emission characteristics and economy of 2 National VI emission standard buses and 2 National III emission standards buses with different fuels for combustion [26]. Zhang *et al.* employed a portable emission testing system to track and detect three diesel buses with diesel oxidation catalysts (DOCs), catalyzed diesel particulate filters (CDPFs) and DOC-CDPFs [27]. Zhang *et al.* applied different PEMSs in the environmental to study the consistency of the emission results for heavy-duty diesel vehicles [28]. Ge *et al.* utilized a PEMS to test the practical road driving emissions of 5 lightweight taxis and 6 heavy urban buses [18].

A study of domestic and foreign literature has revealed that some progress has been made in the study of vehicle PEMS tests in China. However, research in other countries surpasses research in China, and there is still a lack of research on actual road driving emissions for vehicles based on the China VI emission standards. In particular, analyses of the emission characteristics of vehicle pollutants based on the China VI engine standards are needed. This paper emphasizes investigating the PEMS emission characteristics of the China VI emission standards; develop a test scheme that is consistent with the China VI standards; analyzing the emission factors based on the unit mass of fuel, unit road haul and unit time; and monitoring the operation of disposal systems and control strategies for practical roads. The research results provide a reference for the China VI emission standards for vehicle emission factors.

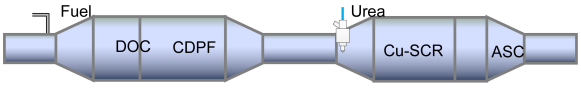

FIGURE 1. Control device for the exhaust pollutants of diesel engines.

II. POLLUTANT CONTROL TECHNOLOGY

Figure 1 is a control device for the exhaust pollutants of diesel engines based on the China VI standards. The device consists of a DOC, DPF, selective catalytic reduction (SCR) device and ammonia slip catalyst (ASC) [29]–[31]. DOCs are usually employed in diesel engine exhaust after a treatment system is utilized. Platinum (Pt), palladium (Pd) and other precious metals are coated as catalysts to reduce the soluble organic matter (SOM) in PM emissions. The conversion efficiency of the DOC is greater than 90% [32]–[34]. The DPF is the most effective diesel engine exhaust particulate capture technology that has been recognized internationally. For the China VI standards, the DPF is installed upstream of the SCR device. The advantage is that the upstream DPF can realize continuous passive regeneration by using doc-transformed NO_2, reducing the frequency of the DPF active regeneration, and improving the fuel economy of diesel engines [35]–[37]. SCR is one of the most effective methods of reducing NO_x pollutants in diesel engine exhaust, and the average conversion efficiency of SCR is approximately 90%–95%. The downstream SCR can apply the upstream doc-converted NO_2 to improve the rapidity of the SCR response and then improve the low-temperature conversion efficiency of SCR [38]–[40]. The ASC can effectively reduce excessive ammonia injection, and the conversion efficiency is generally greater than 90% [40]–[42]. This technical scheme is mainly applied to heavy-duty vehicles that combine urban and high-speed sections [25], [43], [44].

III. TESTING EQUIPMENT AND METHODS

A. TESTING EQUIPMENT

A diesel vehicle practical road emission test was conducted by selecting an aftertreatment system testing vehicle based on the China VI standards and adding a sensor emission technology portable emission equipment (SEMTECH-DS), which is manufactured by the American Sensors company. SEMTECH-DS applied the corresponding model to test air pollutants, such as the instant emissions of CO_2, CO, HC and NO_x. The environmental humidity, temperature, pressure and

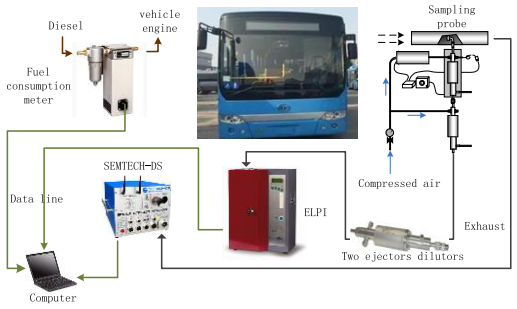

FIGURE 2. Installation diagram of the testing equipment.

other related parameters were also measured. SEMTECH-DS with a GPS can test the vehicle speed and altitude and transmit information to a computer via a USB cable. In addition, before each test, pure nitrogen and standard gas were utilized in zero calibration and alignment by SEMTECH-DS to ensure the accuracy of the measurement results.

An electrical low-pressure impactor (ELPI) was employed for the real-time monitoring of the aerosol particle size distribution and to provide second-by-second PM emission data with a minimum response time of less than 5 seconds. This instrument can measure the airborne particle size distribution in the size range of 7 nm to 10 μm. The instrument should also be zeroed before a test commences.

The two ejector dilutors were installed between the ELPI and the sampling probe. The exhaust gas was diluted by passing compressed air through the dilutors in series before entering the ELPI. The first dilutor was heated to 200°C, and the second ejector dilutor was maintained at room temperature. This approach helped the mixture avoid condensation in the first dilutor and then facilitated cooling in the second dilutor. The dilution ratio during the test was set to approximately 64:1. This ratio has proven to be effective, particularly for inhibiting all post dilution particles that may arise from coagulation and adsorption. Notably, the system was previously employed successfully on many occasions for collecting diesel emission measurements in China.

The general layout of the overall vehicle is shown in Figure 2; it mainly involves the test vehicle, emissions testing equipment, fuel consumption meter and other parts. The major parameters of the overall trial vehicles are displayed in Table 1, and the SEMTECH-DS emission test device measurement range is shown in Table 2. Table 3 gives detailed information about the truncation diameter and median diameter of the ELPI test instrument. Table 4 gives detailed information about the specific parameters of the test fuel.

B. TESTING METHODS

Figure 3 shows the section composition of the test section in the road vehicle PEMS emission test. The trial section follows the road operation condition distribution required by the Chinese VI emission standards, and the vehicle operation road conditions include urban roads, suburban roads, and high-speed sections, which total 45.9 km. By dividing the vehicle operating properties in accordance with the vehicle running speed, the average vehicle velocities are 0–50 km $\cdot h^{-1}$ in the urban section, 50–70 km$\cdot h^{-1}$ in the

TABLE 1. Test vehicle information.

Information	Parameter
Production Enterprise	Suzhou Jinlong
Curb Weight /(kg)	12500
Boundary Dimensions / (mm× mm× mm)	11450×2500×3560
Windward Area / (m^2)	7.74
Drag Coefficient	0.4
Common Speed /($km\cdot h^{-1}$)	100
Maximum Gradient /%	Max Grade ability ≥ 30%
Driving Form	4×2

TABLE 2. SEMTECH-DS measurement range.

Pollutant	Measurement Range	Resolution Ratio	Measurement Accuracy
CO_2	0~20%	0.01%	±3%
CO	0~8%	10×10^{-6}	±3%
HC	0~1000 $\times10^{-6}$	1×10^{-6}	±2%
NO	0~2500 $\times10^{-6}$	1×10^{-6}	±3%
NO_2	0~500$\times10^{-6}$	1×10^{-6}	±3%

TABLE 3. Truncation diameter and median diameter level of ELPI.

Level	D 50%/um	Di/um	ρ/g/cm^3
1	0.0070	0.0214	1.20
2	0.0290	0.0407	1.00
3	0.0570	0.0759	0.85
4	0.1010	0.1291	0.75
5	0.1650	0.2051	0.70
6	0.2550	0.3166	0.60
7	0.3930	0.5003	0.50
8	0.6370	0.7941	0.40
9	0.9900	1.2625	0.35
10	1.6100	1.9901	0.30
11	2.4600	3.1251	0.20
12	3.9700	6.3479	0.10

TABLE 4. Specific parameters of the test fuel.

Parameters	Value	Test method
Sulfur Content/$\times10^{-6}$	10	GB/T 19147-2016
Calorific Value/MJ$\cdot kg^{-1}$	42.77	GB/T 384-1988
Cetane Value	51	GB/T 19147-2016
Density/20℃ ($kg\cdot m^{-3}$)	841	GB/T 19147-2016
Kinematic Viscosity /20℃ ($mm^2\cdot s^{-1}$)	4	GB/T 19147-2016
Carbon Content/%	85.95	SH/T 0656-1998
Hydrogen Content/%	13.39	SH/T 0656-1998
Oxygen Content/%	<0.2	ASTM D5622-95
Ash/%	0.01	GB/T 19147-2016

FIGURE 3. Heavy-duty diesel vehicle PEMS test section.

suburb section and more than 75 km·h^{-1} in the high-speed section. For M_3-type vehicles, the laws pose 70% requirements for the urban section, 30% for the suburb and high-speed sections and within ±10% for deviation control. M_3-type vehicles are defined as a maximum design gross mass more than 5000 kg and capacity of seating more than nine persons.

C. DATA TREATMENT

To directly express the emission levels of pollutants, emission factors are introduced based on the following equations.

The first expression is the emission factor based on fuel consumption [45], namely, the vehicle emission pollutant quantity per unit mass of fuel. Formula (1) adopts the carbon balance method to calculate the emission factor based on the fuel, and the method assumes that all carbon emissions as HC, CO and CO_2. Compared with the gaseous carbon in gas emissions, the carbon in this case is a very small fraction that can be disregarded.

$$Q_{\mathrm{EF}} = \frac{\sum(\rho_{\mathrm{P}} Y Q)}{\sum(\rho_{\mathrm{D}} R_{\mathrm{FC}})} \tag{1}$$

where Q_{EF} is based on the fuel consumption emission factor, g·kg^{-1}; ρ_{P} is the exhausting density in standard conditions, g· m^{-3}; Y is the exhaust volume percentage, m^3·s^{-1}; Q is the exhausting flow in standard conditions, R_{FC} is the specific fuel consumption rate, L·s^{-1}; and ρ_{P} is the fuel density, g·m^{-3}. The exhausting volume flow rate can be calculated by formula (2).

$$Q_{\mathrm{VF}} = \frac{1\,000 R_{\mathrm{FC}} \rho_{\mathrm{D}} R_{\mathrm{CWF}}}{0.866 Y\mathrm{HC}\rho_{\mathrm{HC}} + 0.429 Y_{\mathrm{CO}}\rho_{\mathrm{CO}} + 0.273 Y\mathrm{CO_2}\rho_{\mathrm{CO_2}}} \tag{2}$$

where Q_{VF} represents the exhausting volume, L·s^{-1}; R_{CWF} is the carbon quality percentage in the diesel, 87.98%; φ and ρ represent the mass percentage, $\times 10^{-6}$; and the gas standard density, for example, the volume percentages of HC, CO and CO_2 are 0.866, 0.429 and 0.273, respectively. The diesel densityρ_{D} is 0.996 kg·L^{-1}.

The second high-speed way is the emission factor on account of the real driving emission [46], namely, the vehicle emission pollutant quality of the consuming unit distance (g·km^{-1}). Formula (3) expresses the emission factor based on real driving.

TABLE 5. Fuel-based emission factors.

Model	Speed Range	CO	HC	NO_x
	km·h^{-1}	g·kg^{-1}	g·kg^{-1}	g·kg^{-1}
M_3 Vehicle	Urban	0.39	0.59	1.04
	Suburb	0.19	0.01	0.34
	Highway	0.12	0.00	0.52

$$\mathrm{EF}_{(g/km)} = \frac{\sum \mathrm{ED}}{\sum \mathrm{D}} \tag{3}$$

where ED is the certain pollutant emission velocity of the vehicle per second, and D is the speed per second in the road conditions; the unit is km · s^{-1}.

The third expression is the emission factor based on the time, which is the emission pollutant quantity within the driving unit time, g·s^{-1} [47]. This factor is the instant emission, which is the pollutant emission rate in certain operating conditions.

The error analysis [48] adopts the standard deviation formula (4):

$$\sigma = \sqrt{\frac{1}{N}\sum_{i=1}^{N}(x_i - \mu)^2} \tag{4}$$

where σ is the standard deviation; N is the total number of samples; i is the serial number of samples; X_i is the value of the i sample; and μ is the arithmetic mean.

IV. SIMULATION TEST AND ANALYSIS

To verify the emission characteristics of vehicles in different working conditions, experiments were carried out in urban, suburban and high-speed sections, and NO_x, CO and HC pollutants were measured in real time.

A. EMISSION FACTOR BASED ON FUEL CONSUMPTION

Table 5 shows the emission factors of urban, suburban and high-speed working conditions based on fuel consumption. As shown in Table 5, the CO and HC gaseous pollutants based on fuel consumption decreased with an increase in vehicle speed, engine speed and load. The exhaust temperature remained high, and the aftertreatment DOC effectively oxidized the CO and HC pollutants. The NO_x gaseous pollutant emission factor based on fuel consumption initially decreased and then increased as the driving road conditions changed; the major reason for this trend was the low vehicle exhaust temperature for urban roads. In addition, some low-load working-condition SCR devices may not work normally, which produces a relatively high NO_x pollutant level. For the suburban road and high-speed sections, the pollutant emission amount was large but the exhaust temperature increased, which reduced NO_x pollution.

B. EMISSION FACTOR BASED ON ROAD HAUL

The emission factor based on the road haul adopts an equal-interval separation method for vehicle speeds, where 10 km/h

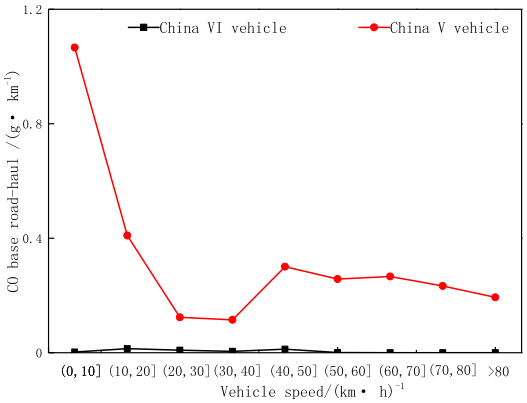

FIGURE 4. CO emission factor comparison based on the road haul.

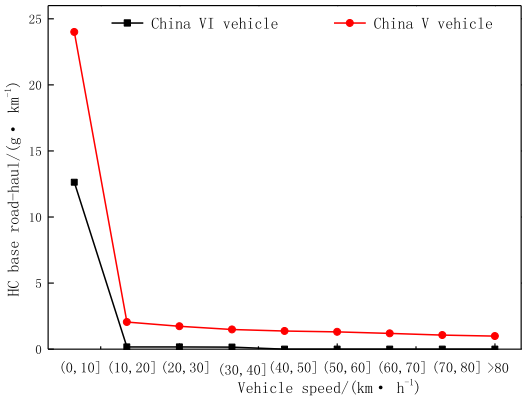

FIGURE 5. HC emission factor comparison based on the road haul.

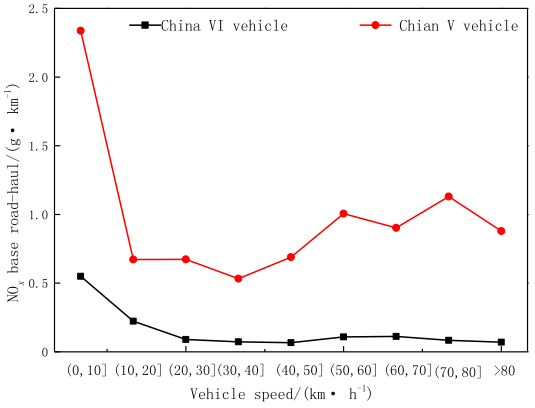

FIGURE 6. NO emission factor comparison based on the road haul.

is the separation interval. The speed is divided into 9 different bins, namely, (0, 10], (10, 20], (20, 30], (30, 40], (40, 50], (50, 60], (60, 70], (70, 80], and (>80]. A weighted average treatment is adopted for all speed intervals to calculate the overall influence of the vehicle emission factor on all speed intervals, and the results are listed in Figures 4-7. The NO, NO_x, CO and HC average emission factors based on the road haul at different speed intervals are given. In the (0, 10] speed interval, the NO, NO_x, CO and HC emission factors are the highest based on the road haul. The pollutant emission factor

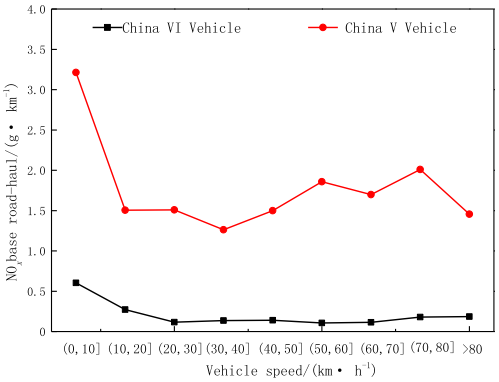

FIGURE 7. NO_x emission factor comparison based on the road haul.

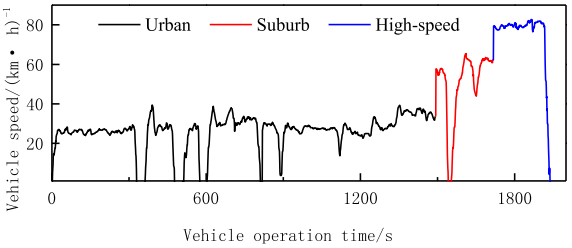

FIGURE 8. Instantaneous vehicle speed for the different operating modes of China VI vehicles.

decreases with an increase in speed. When the speed reaches (20, 30], the emission factor remains relatively stable. The pollutant emission level of China VI heavy-duty vehicles is obviously lower than that of China V vehicles because of the installation of the aftertreatment system. In addition, NO_x decreased by an average of 88%, CO declined by 98% on average, and HC decreased by 62.7% on average. Additionally, NO_x and CO declined greatly, while the decrease in HC was relatively small. As the vehicle starts to accelerate, more fuel oil is injected into the air cylinder immediately, and imperfect combustion occurs in the exhaust with the tail gas in the range of (0, 10]. Moreover, the aftertreatment exhaust temperature is low, and the pollutant conversion efficiency is not high. In this range, after weighting, the proportion of pollution emissions increases. When the speed velocity surpasses 20 km/h, the HC pollutant emission amount decreases considerably, and the emission amount is near zero.

C. EMISSION FACTOR BASED ON THE UNIT TIME

To comprehensively understand the instant emission situation for the China VI emission standards, Figures 8-11 show the vehicle speed versus the NO_x, CO, HC pollutant instant emission rates for the urban road, suburban road and high-speed sections. Vehicle operate the urban road, suburban road and high-speed sections with average proportions of 83.5%, 78.3% and 63.7%, respectively. The average proportions of acceleration and deceleration are 15.8%, 18.5% and 23.8%, respectively. In addition, there is a certain percentage of idling conditions, the average ratio of which is 0.7%, 3.2% and 12.5%, respectively. The test vehicle run speed is relatively low and often involves stopping and driving in the

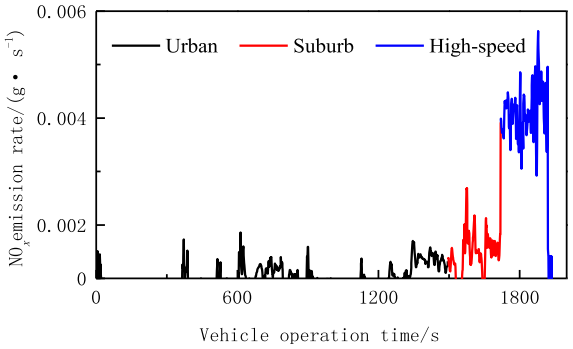

FIGURE 9. NO_X instantaneous emission factors for the different operating modes of China VI vehicles.

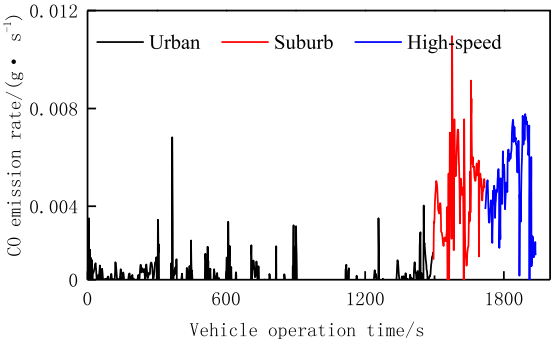

FIGURE 10. CO instantaneous emission factors for the different operating modes of China VI vehicles.

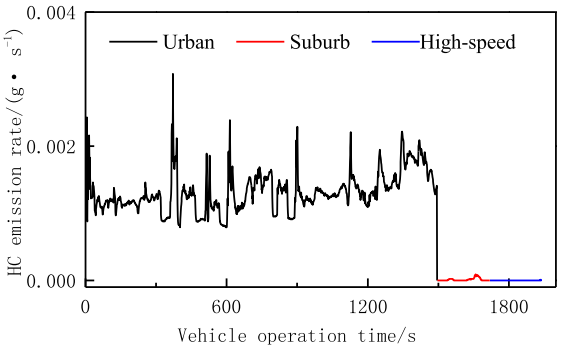

FIGURE 11. HC instantaneous emission factors for the different operating modes of China VI vehicles.

urban road section. On the suburban road section, the average vehicle speed exceeded 50 km/h, and the expressway average speed surpassed 75 km/h. Because China VI emission standard vehicles include the DOC-DPF-SCR-ASC aftertreatment system, the overall NO_x, CO and HC pollutant emission levels were lower than previous emission levels. The NO_x and CO transient pollutant trends increased with an increase in vehicle speed. However, for the suburban road and high-speed sections, the HC pollutant emission amounts were near zero. The major reason for this trend is that the vehicle runs steadily and the engine in-cylinder combustion level is relatively high; so the HC can be oxidized effectively before emission for tests in the suburban road and high-speed sections. In the urban road section, various

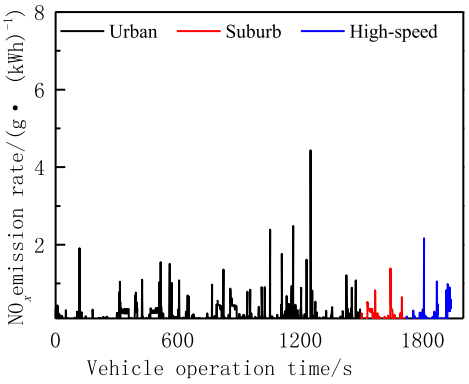

FIGURE 12. NO_X work-based window method emission factor.

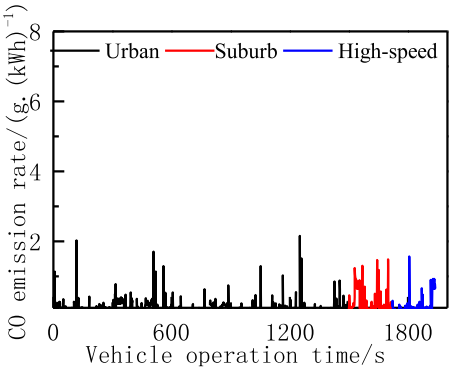

FIGURE 13. CO work-based window method emission factor.

pollutant instant emission rates displayed drastic fluctuations with changes in vehicle acceleration and deceleration. In the suburban road and high-speed road sections, vehicle starting and stopping operations are rare. The emission peaks of HC and CO often appear at vehicle start, stop and acceleration points. These two pollutants are the products of imperfect fuel combustion. During the acceleration process, the fuel injection quantity increases immediately, and the air fuel ratio decreases. Thus, pollutant emissions increase due to imperfect combustion. Because the NO_x emissions are high in the high-speed section, when a vehicle is driving at a high speed, a diesel engine has a high rotation speed and high load, and the engine temperature increases accordingly. Thus, NO_x is generated at a high temperature in an oxygen-enriched environment.

D. EMISSION FACTOR ACCORDING TO THE WORK-BASED WINDOW METHOD

Figures 12-14 show the instant emission factors of NO_x, CO, and HC obtained by the work-based window method weighting. Notably, the integral emission level of NO_x is higher than the HC and CO emission levels. In part of the urban road section, the NO_x emission level is relatively high. The SCR conversion rate is low because vehicles often start and stop in urban areas, which decreases the aftertreatment system exhaust gas temperature lower. Overall, the levels of HC and CO are quite low. In the suburb road and expressway section, the HC emission level is near zero.

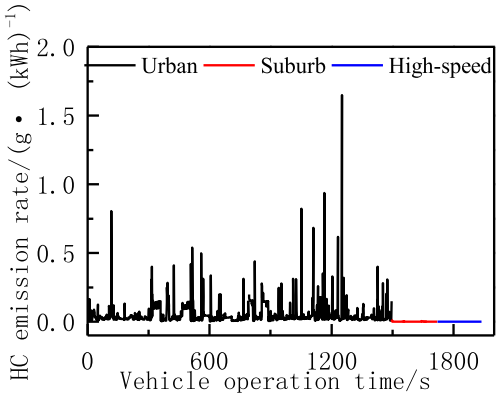

FIGURE 14. HC work-based window method emission factor.

TABLE 6. PEMS emission test results.

Pollutant	Chinese VI Emission Limiting Value (mg·(kWh)$^{-1}$)	Test Result (mg·(kWh)$^{-1}$)
NO_x	690	460
CO	6000	192
HC	—	37.5

The measured exhaust pollutants based on the work-based window method are shown in Table 6. In the urban section, the emission rate of CO pollutants is high because this section has many traffic signals, and the frequent starting and stopping of engines cause the incomplete combustion of fuel injected into the cylinder. The main reason for the high emission rate of NO_x in urban road sections is that the low exhaust temperature of the engine yields the low conversion efficiency of the SCR catalyst. In the high-speed section, the HC emission rate is very low for two reasons: the fuel burns completely in the cylinder with low HC emissions, and the conversion efficiency of HC is high because DOC works in the optimal temperature window. The measurement results for NO_x, CO and HC are 460 mg·(kWh)$^{-1}$, 192 mg·(kWh)$^{-1}$ and 37.5 mg·(kWh)$^{-1}$, respectively. All pollutant levels are lower than the PEMS limiting values, and the test results satisfy the China VI emission standards and requirements.

E. SIZE DISTRIBUTIONS OF PM

Generally, PM emissions are divided into three modes: nucleation mode (condense HC volatiles) with a size range of 10–100 nm; accumulation mode (carbon species and adsorbed material) with a size range of 100–1000 nm; and coarse mode (re-entrained particles) with a size range of 1000–10,000 nm. The average PN and mass size distributions from the three vehicle operation road conditions are depicted in Figures 15-16. PM is the mass of particles, and PN is the number of particles. dM/dlogDp is the mass per unit of particulate size, and dN/dlogDp is the number of particles per unit of particulate size range. PN is concentrated in the range of particle size less than 100 nm. The peak value of the particle size distribution of PN concentration

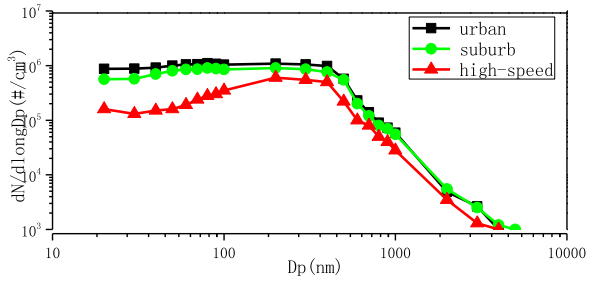

FIGURE 15. Average particle number distributions for the different operating modes of China VI vehicles.

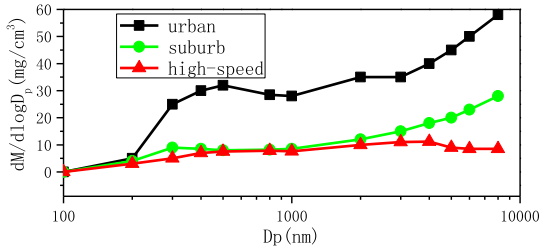

FIGURE 16. Average particle mass distributions for three vehicle operation road conditions.

is 56 nm. The majority of the particles are in the size range 10–100 nm; approximately 88%–95% of the particles are in the size range 10–100 nm; and the fewest particles are in the size range 2000–10,000 nm, which represents approximately 0.08%–0.13% of the total particle mass. The number of particles in different size classes displays the same trend for the three vehicle operation road conditions. These particles, which are formed in nucleation mode and accumulation mode, are composed of condensed hydrocarbon volatiles, carbon species and adsorbed material, which influence human health and air quality.

The experimental results show that the DPF system has a better filtering effect on small-sized particles. In the range of particle size, the diffusion trapping mechanism is dominant, and Brownian motion of particles with small particle sizes is more intense. Therefore, the filtration efficiency is higher.

V. CONCLUSION

In this work, the characteristics of the China VI heavy-duty vehicle emissions were investigated. The relevant conclusions drawn from this study can be summarized as follows:

Based on the actual road emission characteristics of China VI heavy-duty diesel vehicles tested by PEMS, NO_x and HC are higher in urban sections than suburban and high-speed sections because the speeds, exhaust temperatures, and conversion efficiency of the aftertreatment system for pollutants are lower. The gaseous pollutant levels of CO, HC and NO_x for China VI vehicles are significantly lower than those for China V vehicles. The levels of the gaseous pollutants NO_x, HC and CO are significantly lower than those for China V heavy-duty vehicles; notably, the three gaseous pollutants are reduced by 88%, 98% and 62.7%, respectively.

Based on the work-based window method, the data are analyzed. The resulting NO_x measurement is 460 mg·(kWh)$^{-1}$, the CO measurement is 192 mg·(kWh)$^{-1}$, and the HC measurement is 37.5 mg·(kWh)$^{-1}$. The PEM test results for all vehicles satisfy the requirements of the VI regulation.

According to the tests, approximately 88%–95% of the particles are in the 10–100 nm class in the three vehicle operation road conditions and represent approximately 0.08%–0.13% of the total particle mass. These particles, which are formed in nucleation mode and accumulation mode, are mainly composed of condensed hydrocarbon volatiles, carbon species and adsorbed material, which influence human health and air quality.

Additional heavy-duty vehicles based on the China VI standard should be evaluated in further studies to understand the corresponding emission levels. Additional data on heavy-duty vehicle activity and fuel consumption are needed to provide detailed information for developing a heavy-duty vehicle emission inventory in China.

ACKNOWLEDGMENTS

The authors are grateful to the China Environmental Monitoring Center for their cooperation.

REFERENCES

[1] Z. Petranović, T. Bešenić, M. Vujanović, and N. Duić, "Modelling pollutant emissions in diesel engines, influence of biofuel on pollutant formation," *J. Environ. Manage.*, vol. 203, pp. 1038–1046, Dec. 2017.
[2] P. Baskar and A. Senthil Kumar, "Experimental investigation on performance characteristics of a diesel engine using diesel-water emulsion with oxygen enriched air," *Alexandria Eng. J.*, vol. 56, no. 1, pp. 137–146, Mar. 2017.
[3] S. M. Hosseini and R. Ahmadi, "Performance and emissions characteristics in the combustion of co-fuel diesel-hydrogen in a heavy duty engine," *Appl. Energy*, vol. 205, pp. 911–925, Nov. 2017.
[4] P. Geng, E. Cao, Q. Tan, and L. Wei, "Effects of alternative fuels on the combustion characteristics and emission products from diesel engines: A review," *Renew. Sustain. Energy Rev.*, vol. 71, pp. 523–534, May 2017.
[5] S. Vellaiyan and K. S. Amirthagadeswaran, "The role of water-in-diesel emulsion and its additives on diesel engine performance and emission levels: A retrospective review," *Alexandria Eng. J.*, vol. 55, no. 3, pp. 2463–2472, Sep. 2016.
[6] V. Abramesko and L. Tartakovsky, "Ultrafine particle air pollution inside diesel-propelled passenger trains," *Environ. Pollut.*, vol. 226, pp. 288–296, Jul. 2017.
[7] M. Y. Khan, K. C. Johnson, T. D. Durbin, H. Jung, D. R. Cocker, D. Bishnu, and R. Giannelli, "Characterization of PM-PEMS for in-use measurements conducted during validation testing for the PM-PEMS measurement allowance program," *Atmos. Environ.*, vol. 55, pp. 311–318, Aug. 2012.
[8] Z. Chen, X. Wang, Y. Pei, C. Zhang, and M. Xiao, "Experimental investigation of the performance and emissions of diesel engines by a novel emulsified diesel fuel," *Energy Convers. Manage.*, vol. 95, no. 1, pp. 334–341, May 2015.
[9] G. Georgis, M. Filo, A. Thanos, C. Husman, J. C. De L. Ducoing, R. Tafazolli, and K. Nikitopoulos, "SWORD: Towards a soft and open radio design for rapid development, profiling, validation and testing," *IEEE Access*, vol. 10, pp. 186017–186040, 2019.
[10] Z. Liu, Y. Ge, J. Tan, C. He, A. N. Shah, Y. Ding, L. Yu, and W. Zhao, "Impacts of continuously regenerating trap and particle oxidation catalyst on the NO_2 and particulate matter emissions emitted from diesel engine," *J. Environ. Sci.*, vol. 24, no. 4, pp. 624–631, Apr. 2012.
[11] Z. Liu, Y. Ge, K. C. Johnson, A. N. Shah, J. Tan, C. Wang, and L. Yu, "Real-world operation conditions and on-road emissions of Beijing diesel buses measured by using portable emission measurement system and electric low-pressure impactor," *Sci. Total Environ.*, vol. 409, no. 8, pp. 1476–1480, Mar. 2011.
[12] A. Liati, P. D. Eggenschwiler, E. Müller Gubler, D. Schreiber, and M. Aguirre, "Investigation of diesel ash particulate matter: A scanning electron microscope and transmission electron microscope study," *Atmos. Environ.*, vol. 49, pp. 391–402, Mar. 2012.
[13] G. Tian, H. Zhang, Y. Feng, H. Jia, C. Zhang, Z. Jiang, Z. Li, and P. Li, "Operation patterns analysis of automotive components remanufacturing industry development in China," *J. Cleaner Prod.*, vol. 164, pp. 1363–1375, Oct. 2017.
[14] C. T. Lao, J. Akroyd, N. Eaves, and M. Kraft, "Modelling of secondary particulate emissions during the regeneration of diesel particulate filters," *Energy Procedia*, vol. 142, pp. 3560–3565, Dec. 2017.
[15] S. J. Shuai, T. Tang, and Y. G. and Zhao, "Current status and prospects of diesel vehicle emission regulations and aftertreatment technologies," *J. Automot. Saf. Energy.*, vol. 3, no. 3, pp. 200–217, Mar. 2012.
[16] G. D. Tian, Y. Ren, Y. Feng, M. Zhou, H. Zhang, and J. Tan, "Modeling and planning for dual-objective selective disassembly using and/or graph and discrete artificial bee colony," *IEEE Trans. Ind. Informat.*, vol. 15, no. 4, pp. 2456–2468, Apr. 2019.
[17] P. Ju, T. Jiang, H. Li, C. Wang, and J. Liu, "Hierarchical control of air-conditioning loads for flexible demand response in the short term," *IEEE Access*, vol. 7, pp. 184611–184621, 2019.
[18] Y. Ge, A. Wang, M. Wang, Y. Ding, T. Jianwei, and Y. Zhu, "Application of portable emission measurement system (PEMS) on the emission measurements of urban vehicles on-road," *J. Automot. Saf. Energy*, vol. 2, no. 1, pp. 141–145, 2010.
[19] X. B. Shen, Q. D. Wang, and Z. L. Yao, "Study on Road Fuel Consumption Characteristics from Rural Vehicle," *J. Beijing Technol. Bus. Univ. (Natural Sci. Ed.)*, vol. 28, no. 2, pp. 71–75, Feb. 2010.
[20] K. Kaur, N. Kumar, and M. Singh, "Coordinated power control of electric vehicles for grid frequency support: MILP-based hierarchical control design," *IEEE Trans. Smart Grid*, vol. 10, no. 3, pp. 3364–3373, May 2019.
[21] H. K. Wang, L. X. Fu, and A. Z. Chen, "Application of vehicle test system to study the emission characteristics of light motor vehicles on actual roads," *Environ. Sci.*, vol. 29, no. 10, pp. 2970–2974, Oct. 2008.
[22] W. Tian, M. Lauer, and L. Chen, "Online multi-object tracking using joint domain information in traffic scenarios," *IEEE Trans. Intell. Transp. Syst.*, vol. 21, no. 1, pp. 374–384, Jan. 2020.
[23] J. Pielecha, J. Merkisz, and R. Jasiński, "Real driving emissions testing of vehicles powered by compressed natural gas," *SAE paper.*, vol. 3, pp. 18–28, Jan. 2014.
[24] T. Lee, J. Park, S. Kwon, J. Lee, and J. Kim, "Variability in operation-based NOx emission factors with different test routes, and its effects on the real-driving emissions of light diesel vehicles," *Sci. Total Environ.*, vols. 461–462, pp. 377–385, Sep. 2013.
[25] A. M. Fathollahi-Fard, K. Govindan, M. Hajiaghaei-Keshteli, and A. Ahmadia, "A green home health care supply chain: New modified simulated annealing algorithms," *J. Cleaner Prod.*, vol. 240, Dec. 2019, Art. no. 118200.
[26] G. Yong, Q. S. Yu, Y. J. Wang, C. Y. Wang, and Y. Li, "The actual road emission and fuel economy of buses based on different fuels," *J. Environ. Sci.*, vol. 38, pp. 4636–4641, Aug. 2018.
[27] J. Zhang, D. M. Lou, P. Q. Tan, and K. X. Zhao, "Effects of different aftertreatment devices on the reduction of particulate matter in diesel vehicles," *J. Tongji Univ. (Natural Sci.)*, vol. 65, no. 6, pp. 4401–4411, Aug. 2018.
[28] J. Zhang, K. He, Y. Ge, and X. Shi, "Influence of fuel sulfur on the characterization of PM10 from a diesel engine," *Fuel*, vol. 88, no. 3, pp. 504–510, Mar. 2009.
[29] D. Singh, K. A. Subramanian, and M. Garg, "Comprehensive review of combustion, performance and emissions characteristics of a compression ignition engine fueled with hydroprocessed renewable diesel," *Renew. Sustain. Energy Rev.*, vol. 81, no. 2, pp. 2947–2954, Feb. 2018.
[30] U. D. Torre, B. P. Ayo, and M. G. Ortiz, "Steady-state NH_3-SCR global model and kinetic parameter estimation for NO_x removal in diesel engine exhaust aftertreatment with Cu/chabazite," *Catal. Today*, vol. 296, pp. 95–104, Nov. 2017.
[31] W. Li, F. Duan, and C. Xu, "Design and performance evaluation of a simple semi-physical human-vehicle collaborative driving simulation system," *IEEE Access*, vol. 7, pp. 31971–31983, 2019.
[32] M. Pietikäinen, A. Väliheikki, K. Oravisjärvi, T. Kolli, M. Huuhtanen, S. Niemi, S. Virtanen, T. Karhu, and R. L. Keiski, "Particle and NOx emissions of a non-road diesel engine with an SCR unit: The effect of fuel," *Renew. Energy*, vol. 77, pp. 377–385, May 2015.

[33] Y. Z. Xi, N. A. Ottinger, and Z. G. Liu, "New insights into sulfur poisoning on a vanadia SCR catalyst under simulated diesel engine operating conditions," *Appl. Catal. B, Environ.*, vols. 160–161, no. 1, pp. 1–9, Nov. 2014.
[34] B. Shen, Z. Li, J. Li, X. Kong, L. He, J. Song, and X. Liang, "Development of a 1D urea-SCR system model coupling with wall film decomposition mechanism based on engine bench test data," *Energy Procedia*, vol. 142, pp. 3492–3497, Dec. 2017.
[35] T. Qiu, X. Li, H. Liang, X. Liu, and Y. Lei, "A method for estimating the temperature downstream of the SCR (selective catalytic reduction) catalyst in diesel engines," *Energy*, vol. 68, pp. 311–317, Apr. 2014.
[36] M. Fu, Y. Ge, X. Wang, J. Tan, L. Yu, and B. Liang, "NOx emissions from euro IV busses with SCR systems associated with urban, suburban and freeway driving patterns," *Sci. Total Environ.*, vols. 452–453, pp. 222–226, May 2013.
[37] M. Bendrich, A. Scheuer, and R. E. Hayes, "Unified mechanistic model for Standard SCR, Fast SCR, and NO_2 SCR over a copper chabazite catalyst," *Appl. Catal. B, Environ.*, vol. 222, no. 23, pp. 76–87, Mar. 2018.
[38] A. R. Fahami, I. Nova, and E. Tronconi, "A kinetic modeling study of NO oxidation over a commercial cu-CHA SCR catalyst for diesel exhaust aftertreatment," *Catal. Today*, vol. 297, pp. 10–16, Nov. 2017.
[39] Y. Koh, H. Her, K. Yi, and K. Kim, "Integrated speed and steering control driver model for vehicle–driver closed-loop simulation," *IEEE Trans. Veh. Technol.*, vol. 65, no. 6, pp. 4401–4411, Jun. 2016.
[40] M. Chun, C. S. Yoon, and H. Kim, "Basic study on the chemical method for the prevention of recombination in gas produced from decomposition of ammonium carbamate to the solid SCR in a diesel engine," *Trans. Korean Soc. Mech. Eng.-B*, vol. 41, no. 12, pp. 785–793, Dec. 2017.
[41] C. S. Cheng and H. Zhao, "Determination of emission factors of motor vehicles from on-road emissions measurement," *Trans. CSICE*, vol. 34, no. 2, pp. 102–106, Feb.1999.
[42] I. D. Vlieger, D. D. Keukeleere, and J. G. Kretzschmar, "Environmental effects of driving behaviour and congestion related to passenger cars," *Atmos. Environ.*, vol. 34, no. 27, pp. 4649–4655, Dec.2000.
[43] N. Daroogheh, N. Meskin, and K. Khorasani, "Ensemble Kalman filters for state estimation and prediction of two-time scale nonlinear systems with application to gas turbine engines," *IEEE Trans. Control Syst. Technol.*, vol. 27, no. 6, pp. 2565–2573, Nov. 2019.
[44] Y. Jiang, W. Deng, J. Wu, S. Zhang, and H. Jiang, "Adaptive steering feedback torque design and control for driver–vehicle system considering driver handling properties," *IEEE Trans. Veh. Technol.*, vol. 68, no. 6, pp. 5391–5406, Jun. 2019.
[45] T. Lee, J. H. Park, and S. Kwon, "Variability in operation-based NOx emission factors with different test routes, and its effects on the real-driving emissions of light diesel vehicles," *Sci. Total Environ.*, vols. 461–462, no. 1, pp. 377–385, Sep. 2013.
[46] Y. S. Liu, Y. S. Ge, J. W. Tan, M. L. Fu, A. N. Shah, L. Q. Li, Z. Ji, and Y. Ding, "Emission characteristic of off-shore fishing ships of Yellow Bo Sea, China," *J. Environ. Sci.*, vol. 65, no. 3, pp. 83–91, Jul. 2018.
[47] C. He, Y. Ge, C. Ma, J. Tan, Z. Liu, C. Wang, and L. Yu, "Emission characteristics of a heavy-duty diesel engine at simulated high altitudes," *Sci. Total Environ.*, vol. 409, no. 17, pp. 3138–3143, Jul. 2011.
[48] H. Huo, Z. Yao, Y. Zhang, X. Shen, and Q. H. Zhang, "On-board measurements of emissions from diesel trucks in five cities in China," *Atmos. Environ.*, vol. 54, no. 7, pp. 159–167, Jul. 2012.
[49] A. J. Kean, R. F. Sawyer, and R. A. Harley, "A fuel-based assessment of off-road diesel engine emissions," *J. Air Waste Manage. Assoc.*, vol. 50, no. 11, pp. 1929–1939, Jun. 2000.

YINGSHUAI LIU received the B.S. degree in optical information science and technology and the M.S. degree in optical engineering from the Ocean University of China, Qingdao, China, in 2005 and 2009, respectively, and the Ph.D. degree in power machinery and engineering from the Beijing University of Technology, Beijing, China, in 2019.

He is currently a Lecturer with the Weifang University of Science and Technology. He is currently engaged in postdoctoral research by joint training with Southwest Jiaotong University and Ningbo Free Trade Zone. He has published over ten journal articles and conference proceedings papers in his research areas such as the IEEE Transactions on Automation Science and Engineering, *Computers and Chemical Engineering*, and *Computers and Industrial Engineering*. His research interests include engine energy saving and emission reduction, green manufacturing, green logistics and transportation, intelligent inspection and repair of automotive, decision making and intelligent optimization, facility location, and prediction and assessment for economic and environment.

JIANWEI TAN received the B.S. degree in computer and applications from the Ocean University of China, Qingdao, China, in 2001, and the M.S. degree in power machinery and engineering and the Ph.D. degree in environmental engineering from the Beijing Institute of Technology (BIT), Beijing, China, in 2004 and 2007, respectively. He was a Visiting Scholar with Cornell University, from 2012 to 2013. He joined the BIT, in 2007, and is currently an Associate Professor of internal combustion engine engineering. He has over 90 publications. His research interests are in vehicle emission, sensor networks, big data, and transportation and energy systems. He is the Evaluation Expert of the National Natural Science Foundation of China. He is a Motor Vehicle Review Expert from Beijing Eco-Environmental Bureau.